



Article

Synergistic Effect in MoS₂ Nanosheets–Biochar Nanocomposites with Enhanced Surface Area and Electrical Conductivity for Energy Storage Applications

Thangaraj Pandiselvi ¹, Chithiraiselvan Praveena ¹, Venkatachalam Sridevi ^{1,*} , Balu Alagar Venmathi Maran ^{2,*} and Masanari Kimura ³

¹ Department of Chemistry, Lady Doak College, Madurai 625 002, Tamil Nadu, India; pandiselvi ldc@gmail.com (T.P.); praveenachithiraiselvan@gmail.com (C.P.)

² Graduate School of Integrated Science and Technology, Nagasaki University, 1–14 Bunkyo-machi, Nagasaki 852-8521, Japan

³ Graduate School of Engineering, Nagasaki University, 1-14 Bunkyo-machi, Nagasaki 852-8521, Japan; masanari@nagasaki-u.ac.jp

* Correspondence: sridevi@ldc.edu.in (V.S.); bavmaran@nagasaki-u.ac.jp (B.A.V.M.); Tel.: +81-70-9279-6123 (B.A.V.M.)

Abstract: Layered molybdenum disulfide (MoS₂), a transition metal dichalcogenide, shows distinct optical, electrical, and physical properties at a few-layer thickness. MoS₂ nanosheets (NSs) widely explored for energy and environmental applications but have limitations with respect to their electrical conductivity and charge transfer characteristics due to their low surface area. These limitations can be overcome by combining MoS₂ NSs with carbon-based materials like graphene, carbon nanotubes, and biochar, which can enhance the properties in a synergistic way. In this study, biochar (BC), a carbon-rich material prepared from vegetable biomass through low-temperature pyrolysis has been combined with bulk MoS₂ in various ratios using an aqueous phase exfoliation method to form MoS₂ NSs–biochar nanocomposites. The spectroscopic, structural, and morphological studies confirmed the synergistic interaction between MoS₂ and BC, which is well reflected in the facile exfoliation process and the formation of few layered MoS₂ NSs on the surface of the BC without any agglomeration. The electrochemical studies prove that incorporating biochar into MoS₂ enhances the capacitive behavior and reduces the charge transfer resistance compared to pristine MoS₂ NSs and pristine biochar. This study provides ample scope for the composite to be explored for energy storage applications, especially towards the development of electrode materials due to the synergistic effect between MoS₂ NSs and biochar.

Keywords: MoS₂ nanosheets; biochar; nanocomposites; xsupercapacitors; exfoliation; energy storage



Citation: Pandiselvi, T.; Praveena, C.; Sridevi, V.; Venmathi Maran, B.A.; Kimura, M. Synergistic Effect in MoS₂ Nanosheets–Biochar Nanocomposites with Enhanced Surface Area and Electrical Conductivity for Energy Storage Applications. *J. Compos. Sci.* **2024**, *8*, 357. <https://doi.org/10.3390/jcs8090357>

Academic Editor: Mohd Shahneel Saharudin

Received: 6 August 2024

Revised: 28 August 2024

Accepted: 10 September 2024

Published: 12 September 2024



Copyright: © 2024 by the authors. Licensee MDPI, Basel, Switzerland. This article is an open access article distributed under the terms and conditions of the Creative Commons Attribution (CC BY) license (<https://creativecommons.org/licenses/by/4.0/>).

1. Introduction

Transition metal dichalcogenides (TMDs) are a class of layered two-dimensional materials such as MoS₂, MoSe₂, WS₂, WSe₂, TaS₂, TiS₂, and NbS₂, which have received greater attention due to their unique properties like a high surface area, electron mobility, strong light–matter interactions, and thermal conductivity [1]. In particular, layered MoS₂ nanosheets (NSs), which contain S–Mo–S layers with weak interlayer van der Waals interaction and strong intralayer covalent bonds, possess high mechanical strength, and tunable electronic, optical, and electrochemical properties. In addition, MoS₂ NSs can also act as electrode materials in energy storage devices because of their variable oxidation states ranging from +2 to +6 [2]. However, pristine MoS₂ NSs face challenges such as aggregation and restacking of layers that decrease the surface area, which hampers efficient electron transfer and results in limited electrical conductivity in energy storage applications [3]. To overcome these limitations, MoS₂ can be combined with suitable counter materials

such as carbon-based materials, polymers, biopolymers, metal oxides, and sulfides [4] to enhance the surface area and electrical conductivity of MoS₂, thereby enhancing its electrochemical performance.

Among the various counter materials that are added to MoS₂, carbon-based materials such as graphene, reduced graphene oxides, carbon nanotubes, and carbon nanofibers, are considered to be ideal as these materials exhibit distinct properties such as a porous structure and large surface area, which improves the electrochemical properties of pristine MoS₂ [5]. There are several reports on MoS₂/carbon-based composites such as MoS₂/carbon, MoS₂/graphene, MoS₂/graphene oxide, MoS₂/reduced graphene oxide, MoS₂/carbon nanotubes, MoS₂/carbon nanofibres, and MoS₂/graphitic carbon nitrides for various applications like photocatalytic degradation, biosensors, energy conversion, and storage applications [6–9]. In the recent past, combining carbon materials derived from biosources with MoS₂ has gained interest due to its eco-friendly approach to converting biowaste to a value-added product for suitable applications. The incorporation of carbon-based materials such as nanocomposites into MoS₂ can be considered an environmentally sustainable method compared to conventional carbon-based materials like graphene or carbon nanotubes [10] which involve hazardous chemicals, high cost, complex synthesis procedures, and limited scalability.

The carbon derived from different biosources such as agricultural waste, forestry residues, animal wastes, municipal solid waste and industrial waste is referred to as biocarbon, activated carbon, or biochar depending on the method of preparation. Biochar (BC) is a highly porous and carbon-rich material with large surface area and high electrical conductivity, derived from different biomass through pyrolysis under low oxygen atmosphere [11]. It has been identified as a suitable material to combine with MoS₂ to offset its limitation. Upon combining MoS₂ with BC, the properties of the resulting nanocomposite (NC), such as material stability, surface area, electrical conductivity, and specific capacitance, are found to increase, enabling the composite material to be suitable for electrochemical applications, especially in the field of energy storage. Zhao et al. [12] successfully synthesized MoS₂/carbon using corn stalks as a biocarbon source, which resulted in the formation of NCs with large surface area, high specific capacitance, and good stability when used as an anode material in supercapacitors. Sangeetha and Selvakumar [13] utilized biomass from Tendu leaves and polyethylene terephthalate bottles to produce activated carbon, which was then used to prepare an MoS₂/activated carbon composite for supercapacitor applications. The sponge-like activated carbon network, with a thin layer of molybdenum disulfide–carbon, demonstrated a high power density. Khandare and their group synthesized an MoS₂ nanobelt–carbon composite using a hydrothermal method in which carbon was derived from a lemongrass (LG) plant through impregnation with KOH and pyrolysis. Their findings indicate that the MoS₂ nanobelts improved the electrochemical properties of LG carbon by enhancing the interaction between the electrolytes and the active electrode material [14]. Mahajan et al. [15] synthesized biocarbon–MoS₂ nanospheres using hydrothermal techniques; the biocarbon was produced from date peels and seeds via pyrolysis, which resulted in improved specific capacitance of the NCs. Wang et al. [16] developed MoS₂ nanoflowers on nanoflakes of biomass-derived carbon and used this as an electrode material which exhibited a low impedance, high specific surface area, and specific capacitance.

Apart from energy storage applications, MoS₂/BC NCs were also synthesized for different applications such as adsorption, photocatalytic degradation of organic pollutants, and water remediation [17–21]. All the reported methods for the preparation of MoS₂/BC NC so far demand a complex bottom-up method for the synthesis of the MoS₂ nanomaterial and high temperature for the activation of biocarbon, thus they are very time consuming. In this paper, we have demonstrated a facile, time-efficient, sustainable, and eco-friendly top-down method for the preparation of a MoS₂/BC NC for the first time through an aqueous phase exfoliation of MoS₂ and BC derived from household vegetable waste. The prepared NC was found to exhibit interesting and superior properties in a synergistic way

compared to pristine MoS₂ NSs and pristine BC, and the findings of the study are presented in the following sections.

2. Materials and Methods

2.1. Materials

The MoS₂ powder was bought from ThermoFisher Scientific Pvt. Ltd., Mumbai, India. Sulphuric acid (H₂SO₄) was purchased from Rankem Pvt. Ltd., Maharashtra, India. All the experiments were conducted using deionized water. All the chemicals were of analytical grade and used without additional purification.

2.2. Preparation of BC

Vegetable biomass was collected from household vegetable waste for the BC preparation. The collected biomass was washed thoroughly with deionized water in order to remove impurities and dried in a hot air oven at 100 °C for 5 h before pyrolysis. The quality of BC depends on the pyrolysis temperature and the oxygen atmosphere. Generally, low-temperature (<300 °C) pyrolysis produces a low carbon content with less stable BC, while high-temperature (350–750 °C) pyrolysis decreases the pore volume and surface area with the increase in ash content [10,11]. Therefore, it is crucial to optimize the temperature for the proper pyrolysis of waste to generate high quality BC. Pyrolysis at low oxygen or no oxygen conditions prevents complete combustion, which allows the organic material to break down to solid char rather than ashes. In our study, the dried samples were subjected to nitrogen (N₂) purging for nearly 30 min to maintain a low oxygen atmosphere, then placed in a muffle furnace and heated to an optimized temperature of 300 °C gradually at a ramp rate of 4 °C per minute. After pyrolysis, the sample was allowed to cool down to room temperature (30 °C) and removed from the furnace. The black-colored solid was crushed to a fine powder using a mortar and pestle, then sieved in a mechanical sieve with a pore size of 75 µm to obtain a uniformly sized BC powder. The finely sieved black powder was then dialyzed using a cellulose ester dialysis membrane of 10 kDa for 24 h in water to remove unwanted ions, and the purified BC was collected and stored for further analysis.

2.3. Preparation of MoS₂/BC NCs

The MoS₂–BC NCs were synthesized via a simple, top-down approach by exfoliating a mixture of bulk MoS₂ and BC powders in different ratios in aqueous solution using an ultrasonication method. Initially, bulk MoS₂ with different amounts of BC in ratios of 10:1, 10:2, and 10:3 (*w/w*) was taken and dispersed in 10 mL of water. Then, the dispersion was ultrasonicated for 2 h using an ultrasonicator (power of 120 W) at an ambient temperature. After the ultrasonication process, the dispersion was transferred into a centrifuge tube and centrifuged at 6000 rpm for 60 min. The clear supernatant liquid was carefully transferred to a centrifuge tube using a micropipette, then further centrifuged to ensure the complete removal of the larger particles in the samples, and stored for further studies. For the comparative studies, bulk MoS₂ and BC were also exfoliated separately for 2 h by adopting the same procedure. The prepared NCs (3 samples) and exfoliated bulk samples (MoS₂ and BC) were labeled as MoS₂/BC1, MoS₂/BC2, MoS₂/BC3, pristine MoS₂ NSs, and pristine BC, respectively, and are indicated using the same labels in the following sections.

2.4. Characterization Techniques

The ultraviolet-visible (UV-Vis) absorption spectra were recorded on a JASCO V-630 UV-Visible spectrophotometer (JASCO International Co., LTD, Tokyo, Japan) using a quartz cell with 1 cm thickness and scanned within a range of 200–800 nm at room temperature. The Raman spectra of the prepared samples were recorded on a modular 1064 Raman system, Bay Spec, CA, USA, in the spectral range of 400–3000 cm^{−1} using a 1064 nm near infra-red laser with a power of 149 mW. The photoluminescence (PL) spectra of the samples were analyzed using a JASCO (FP 8500) spectrofluorometer (JASCO International Co., LTD., Tokyo, Japan) with excitation wavelengths. AFM images were obtained using FEG

Quanta-250 and Nanosurf Easy scans 2 (Nanosurf AG, Switzerland) instruments. For AFM analysis, the as-prepared samples were attached on an AFM stub and images were recorded in static force mode using a ContA1-G probe cantilever, applying a scan rate of 2 Hz. The field emission scanning electron microscopy (FESEM) images and the energy dispersive X-ray (EDX) spectra were obtained using Carl ZEISS EVO 18 and ZEISS smartEDX, (ZEISS, Oberkochen, Germany) respectively. The sample preparation for FESEM and EDX involved drying a droplet of a suspension of the sample on aluminium foil. Afterward, the samples were coated with a thin layer of gold using a sputtering technique, then secured onto the sample stage with conductive double-sided tape. The X-ray diffractometer (XRD) analysis of the samples was obtained with a BRUKER ECO D8 ADVANCE (Bruker Pvt. LTD., Ettlingen, Germany), using Cu K α radiation as an X-ray source ($\lambda = 1.5406 \text{ \AA}$) at room temperature under an operating voltage of 40 kV and a current of 30 mA.

2.5. Electrochemical Studies Using a Modified Glassy Carbon Electrode (GCE)

The GCE surface was 3 mm diameter and was cleaned using 0.3 μm and 0.05 μm of micro polish alumina, rinsed with double distilled water, then ultrasonicated in acetone for one minute. After ultrasonication, the electrode was allowed to dry at room temperature. Then, 5 μL of the prepared samples were drop cast onto the pre-cleaned GCE surface and dried at room temperature. The electrochemical measurements of the samples were performed using a CHI model 660C (Austin, TX, USA) electrochemical workstation in 1 M H_2SO_4 . The experiments were performed using a three-electrode cell set up with a platinum wire as the counter, Ag/AgCl as the reference, and modified glassy carbon as the working electrodes. Cyclic voltammetry (CV) studies were carried out in the range of a 10–100 mV/s scan rate and electrochemical impedance spectroscopic (EIS) studies were in the range of 100 kHz–0.1 Hz at the open circuit potential, with an AC amplitude of 5 mV. The surface areas of the modified electrodes were calculated using the Randles–Ševčík equation, $I_{\text{pa}} = 2.69 \times 10^5 n^{3/2} A C_0 D^{1/2} \nu^{1/2}$; where I_{pa} represents the peak current, n is the number of electrons transferred, A is the surface area of the electrode, C_0 is the concentration of the electroactive species, D is the diffusion coefficient ($6.69 \times 10^{-6} \text{ cm}^2 \text{ s}^{-1}$), and ν is the scan rate. The specific capacitance (C_s) of the prepared material was calculated from the CV curve using the following equation:

$$C_s = \frac{\int_{v_1}^{v_2} I dv}{2m\nu\Delta v}$$

where $\int_{v_1}^{v_2} I dv$ represents the area of the CV curve, m is the mass of the active material in the electrode, ν is the scan rate, and Δv is the operating potential window [22].

3. Results and Discussion

The method of preparing the NCs adopted in our study eliminates the use of hazardous chemicals or solvents and involves a facile exfoliation of the materials in the aqueous phase within a short duration of 2 h (Figure 1). The ultrasonication leverages high-frequency sound waves to create shear forces that exfoliate bulk materials into individual nanosheets [23]. After exfoliation, NCs comprising a few layers of MoS_2 and BC particles were obtained, as revealed by the various characterization studies presented in the following sections.

3.1. UV-Vis Spectroscopic Analysis

The UV-Vis spectrum was recorded for $\text{MoS}_2/\text{BC1}$, $\text{MoS}_2/\text{BC2}$, $\text{MoS}_2/\text{BC3}$ NCs, pristine MoS_2 NSs, and pristine BC. Generally, the absorption spectrum of bulk MoS_2 has four excitonic peaks in the region of 600–700 nm and 400–500 nm, which are designated as A and B and C and D peaks, respectively [24]. As it reduces to few-layered NSs upon exfoliation, the reduction in thickness is indicated by a blue shift of all four peaks and the C and D peaks become resolved. In the exfoliation methods reported earlier, this kind of shift and resolution in the peaks happened after long hours of sonication (8 h) [25]. In

the present study, the formation of few-layered NSs occurred within 2 h, as indicated by the shift and resolution of peaks in the UV-Visible spectrum (Figure 2a) when bulk MoS₂ was exfoliated along with BC. The excitonic peaks of the three NCs (Table 1) exhibited a gradual blue shift of the A and B peaks with peak-to-peak separation of ~62 nm, and well-resolved C and D peaks upon the addition of BC compared to the pristine MoS₂ NSs. An increase in the amount of BC beyond 10:3 in the NCs showed no significant shift in the excitonic peaks; hence, the optimum ratio of MoS₂: BC for the effective exfoliation of MoS₂ was fixed at 10:3. Also, the bulk BC did not show any characteristic peaks in the UV-visible region [26]. Upon exfoliation for 2 h, the absorption peak of pristine BC appeared at 213 nm (Figure 2b), which was ascribed to the presence of aromatic carbon structures [27] in the exfoliated BC. The drastic reduction in the exfoliation time for the formation of NSs clearly indicates that added BC plays a vital role in the formation of NSs. Once the layers of MoS₂ become separated from the bulk by ultrasonication, they are slowly adsorbed on the surface of the BC present in the medium, which prevents the restacking and agglomeration of the formed NSs. Thus, the gradual addition of BC facilitates a facile exfoliation of MoS₂ and enhances the formation of few-layered MoS₂ NSs within a short duration, especially in MoS₂-BC3 NC. Also, the stability of the prepared NC (MoS₂-BC3) was monitored using UV-Vis spectroscopy and the spectrum was recorded over a period of 3 months (Figure 2c). The characteristic peaks of MoS₂ (A, B, C, and D) remained unaltered for one month and exhibited a gradual shift in the peaks thereafter, indicating the agglomeration of the nanosheets.

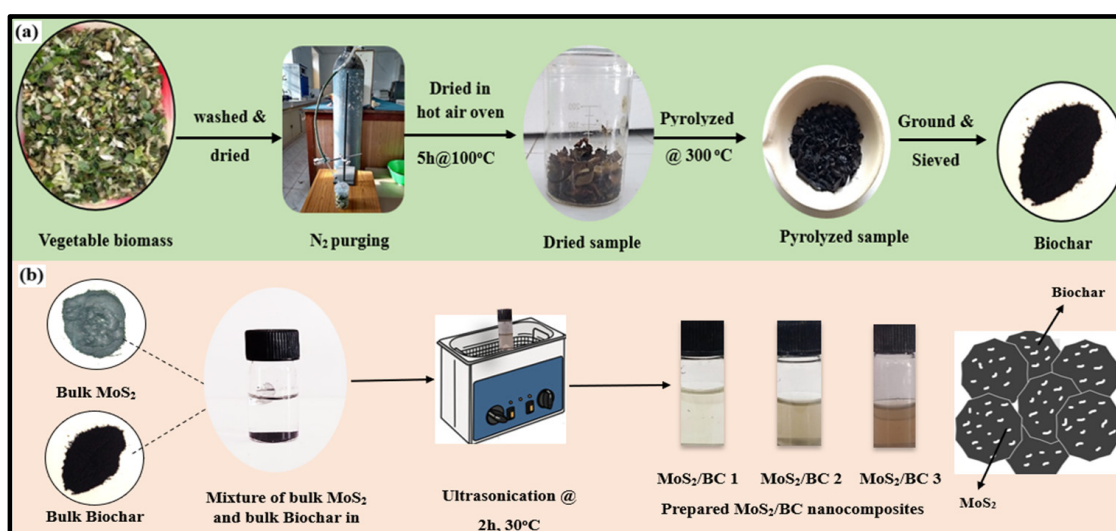


Figure 1. Schematic illustration of preparation of (a) bulk BC and (b) MoS₂/BC NCs.

Table 1. UV-Vis excitonic peaks for the bulk MoS₂, pristine MoS₂ NSs, and the prepared NCs.

Samples	Excitonic Peaks (nm)			
	A	B	C	D
Bulk MoS ₂	690	632	507 (Unresolved single broad peak)	
Pristine MoS ₂ NSs	681	620	468	405
MoS ₂ /BC1	679	619	466	403
MoS ₂ /BC2	679	619	457	402
MoS ₂ /BC3	674	612	453	393

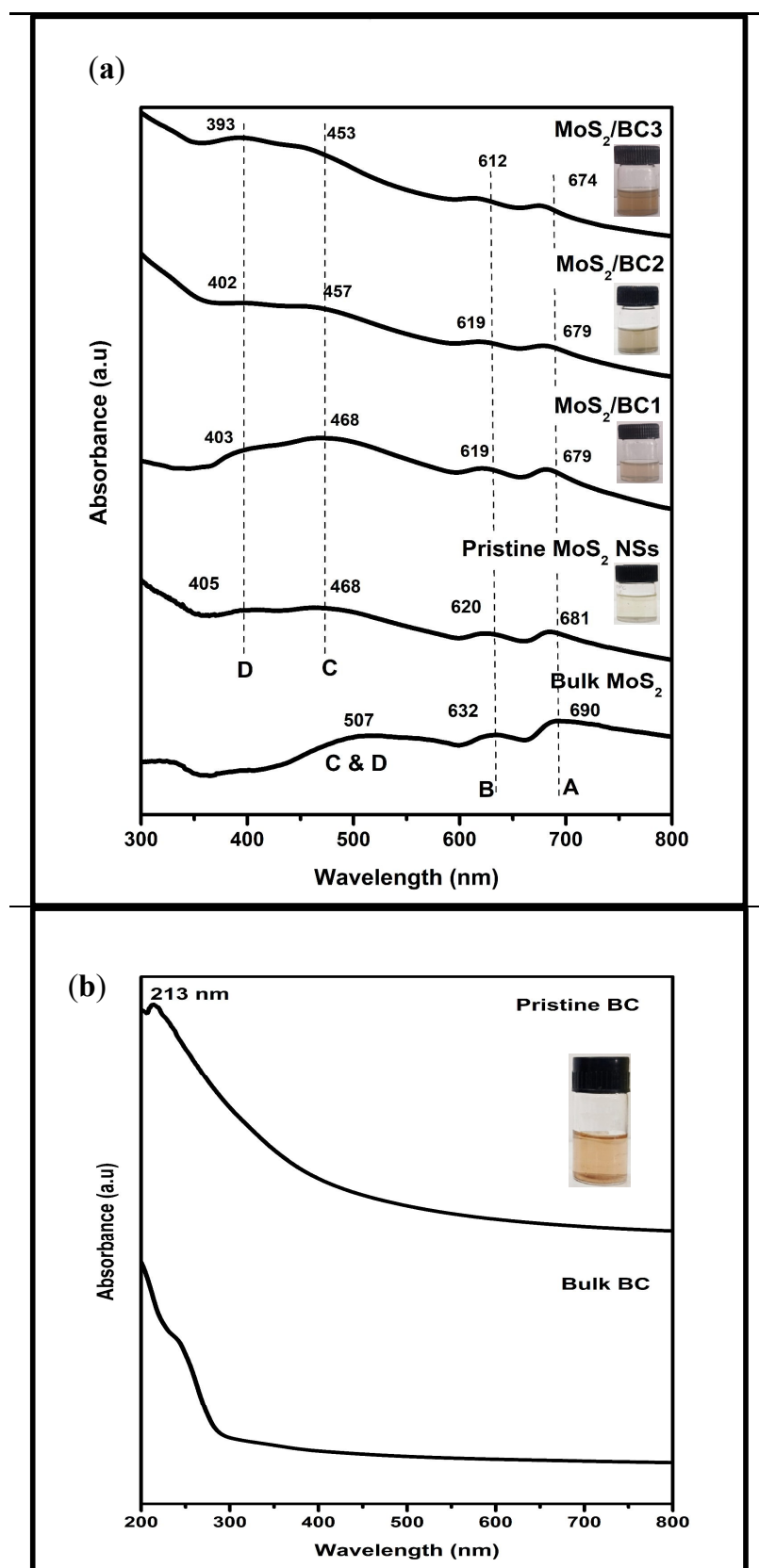


Figure 2. Cont.

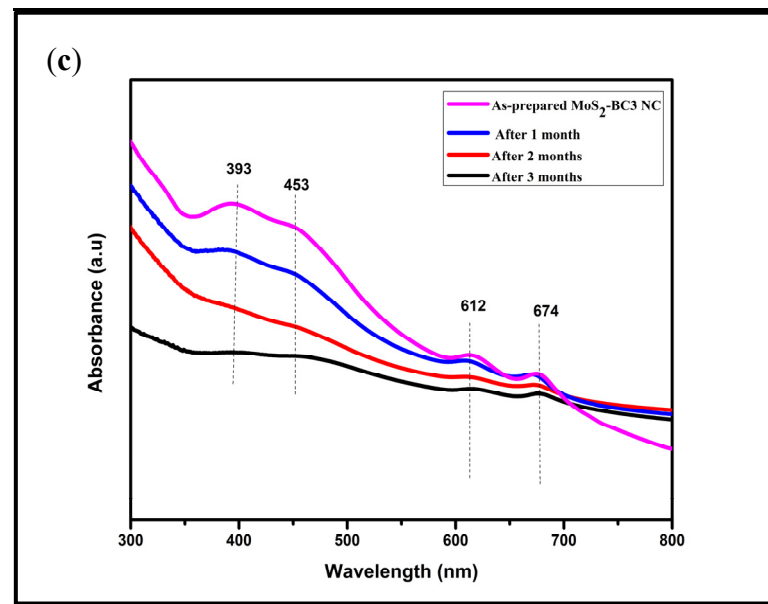


Figure 2. UV-Vis spectra of (a) bulk MoS₂, pristine MoS₂ NSs, MoS₂/BC1, MoS₂/BC2, and MoS₂/BC3 NCs; (b) bulk BC and pristine BC, and (c) stability studies of the prepared MoS₂/BC3 NC.

3.2. Raman Spectroscopic Analysis

Raman spectroscopy was employed to analyze the structural changes and interaction between BC and MoS₂ (Figure 3). The two signature peaks of bulk BC which appear at 1326.9 and 1440.12 cm^{−1} are recognized as the D band and G bands. The D (defective) band is associated with the breathing mode of carbon, which is an indication of the disordered structure of carbon, and the G band corresponds to the in-plane vibrational mode of the sp² hybridized carbon atoms in the BC [28]. Similarly, MoS₂ NSs show two signature peaks at 370.6 and 402.7 cm^{−1}, which correspond to the E_{1g}¹ (in-plane opposing vibrations of Mo and sulfur atoms) and A_{1g} (out-of-plane vibration mode of sulfur atoms) vibrational modes, respectively, confirming the layered structure of MoS₂ [29]. The as-prepared NCs show the presence of the signature peaks of both BC and MoS₂ NSs, with a frequency shift and intensity change in the D and G bands due to the incorporation of MoS₂ into BC. The decrease or increase in the intensity ratio of (I_D/I_G) is a measure of the order or disorder state of the sp² carbon network in the BC. In the prepared NCs, the I_D/I_G ratio increases from MoS₂/BC1 to MoS₂/BC3 compared to pristine BC, which reveals the presence of more disorder in the carbon network due to the adsorption of MoS₂ on the surface of the BC [14]. The observed I_D/I_G ratios for pristine BC, MoS₂/BC1, MoS₂/BC2, and MoS₂/BC3 are 0.23, 0.55, 0.57, and 0.60, respectively. Thus, in MoS₂/BC3 NC, the high I_D/I_G value indicates an effective interaction between the MoS₂ and BC, which helps to tune the properties of the NCs synergistically compared to pristine materials.

3.3. PL Spectroscopic Analysis

The PL spectroscopy was employed to study the quantum confinement effects and the defects present in the prepared samples (Figure 4). The PL spectra for all the samples were recorded at excitation wavelengths corresponding to their ultraviolet absorption peaks. Bulk and pristine MoS₂ NSs did not show any PL emission peaks as reported by [30], whereas bulk and pristine BC with an excitation wavelength of 200 nm exhibited broad emission peaks at 527 and 460 nm due to the presence of structural defects in the extended conjugation of the carbon network. A large redshift with enhanced PL intensity was observed in all the three NCs, MoS₂/BC1, MoS₂/BC2, and MoS₂/BC3, at 432, 453, and 445 nm, respectively, at their corresponding excitation wavelengths of 233, 245, and 254 nm. Hence, with the increase in the amount of BC in the NCs, the PL property also increases, and the increase in the PL intensity indicates the presence of more defect states in the NCs

due to the strain created at the interface of the carbon surface and the MoS₂ NSs [31]. Thus, the luminescence property of pristine BC is very much enhanced in the presence of MoS₂ NSs in the NCs, thus implying the good synergy between BC and MoS₂.

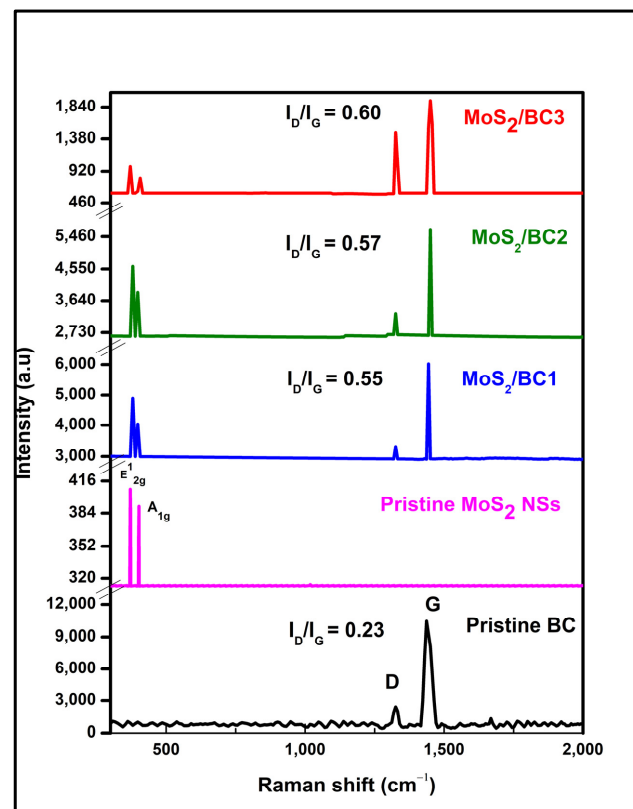


Figure 3. Raman spectra of pristine BC, pristine MoS₂ NSs, MoS₂/BC1, MoS₂/BC2, and MoS₂/BC3 NCs.

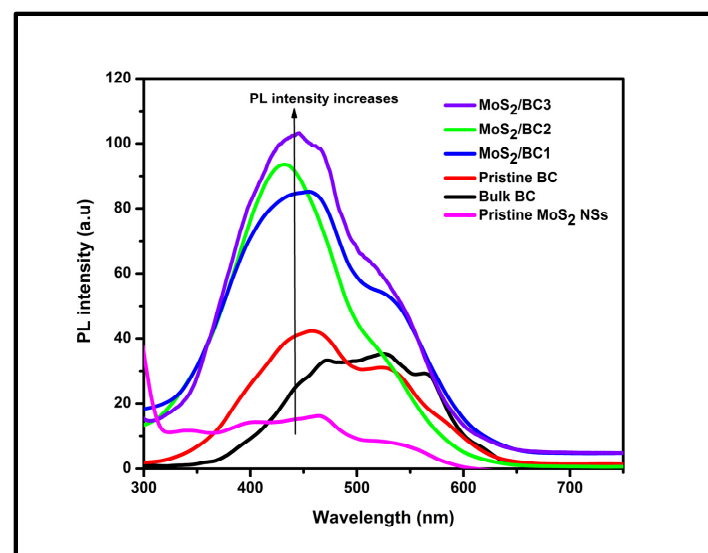


Figure 4. PL spectra of pristine MoS₂ NSs, bulk BC, pristine BC, MoS₂/BC1, MoS₂/BC2 and MoS₂/BC3 NCs.

The spectroscopic analysis clearly revealed that out of the three NCs prepared, MoS₂/BC3 exhibits superior properties; hence, detailed structural and morphological studies were carried out with the MoS₂/BC3 NC, then compared to pristine BC and pristine MoS₂ NSs in the following sections.

3.4. XRD Analysis

The XRD spectrum was recorded for MoS₂-BC3 NC, pristine BC, and pristine MoS₂ NSs (Figure 5). The XRD diffraction patterns of pristine MoS₂ NSs show peaks at 14.38°, 29.01°, 32.54°, 33.63°, 35.78°, 39.59°, 44.21°, 49.90°, and 60.21°, which were assigned to the lattice planes of (002), (004), (101), (103), (006), (105), and (008), respectively [32]. These diffraction peaks are indexed and match well with the hexagonal MoS₂ (JCPDS No. 37-1492). The pristine BC showed two broad peaks at 25.3° and 43.2° due to the presence of an amorphous structure arising from disordered carbon atoms [33], while in MoS₂/BC3 NC, these peaks shifted to 28.01° and 40.69° (Figure 5b) due to the presence of MoS₂ on the surface of the BC. In addition to this, the XRD pattern of the MoS₂/BC3 NC shows the peaks of pristine MoS₂ NSs with a significantly reduced intensity peak of a (002) plane at a lower 2θ value (13.84°) due to the formation of few-layered NSs in the NC. Thus, the amorphous nature of the BC present, along with crystalline MoS₂ NSs, enhances the overall surface area of the prepared NC.

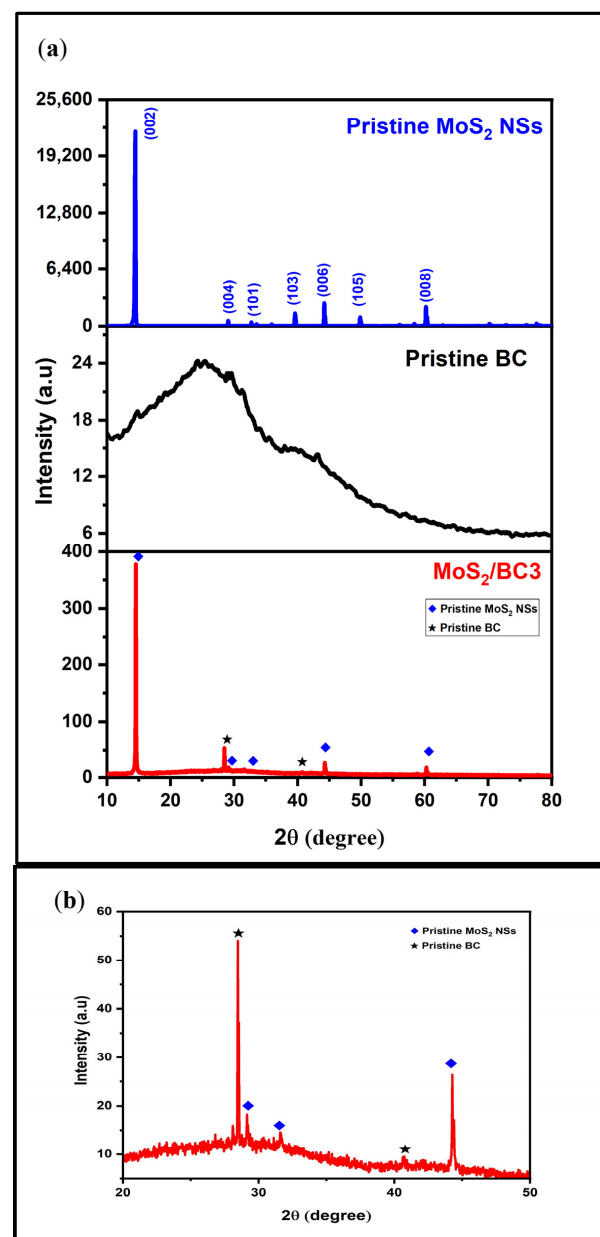


Figure 5. XRD patterns of (a) pristine MoS₂ NSs, pristine BC and MoS₂-BC3 NC; (b) Expanded XRD pattern of MoS₂/BC3 NC (20–50°).

3.5. AFM Analysis

The AFM images of the MoS₂-BC-3 NC, pristine BC, and pristine MoS₂ NSs at two different magnifications are shown in Figure 6a–f. The height profiles (Figure 6g–i) and thickness histograms (Figure 6j–l) clearly show that the layer thickness of the MoS₂-BC-3 NC is significantly reduced compared to pristine MoS₂ NSs and pristine BC, which had bigger and more agglomerated particles after the same 2 h of exfoliation. Hence, the presence of BC is crucial in bringing about the thickness and size reduction in bulk MoS₂ within 2 h.

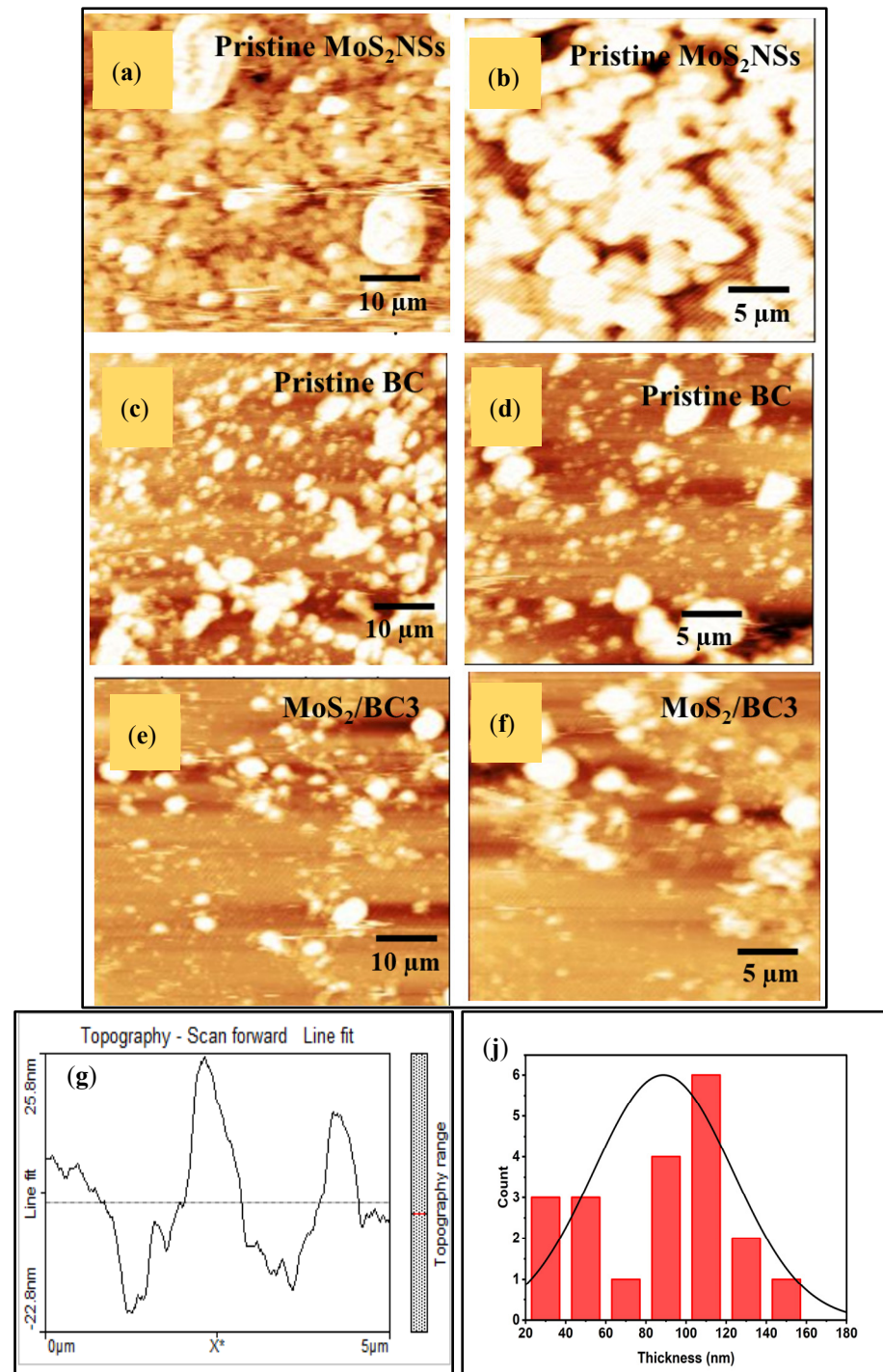


Figure 6. Cont.

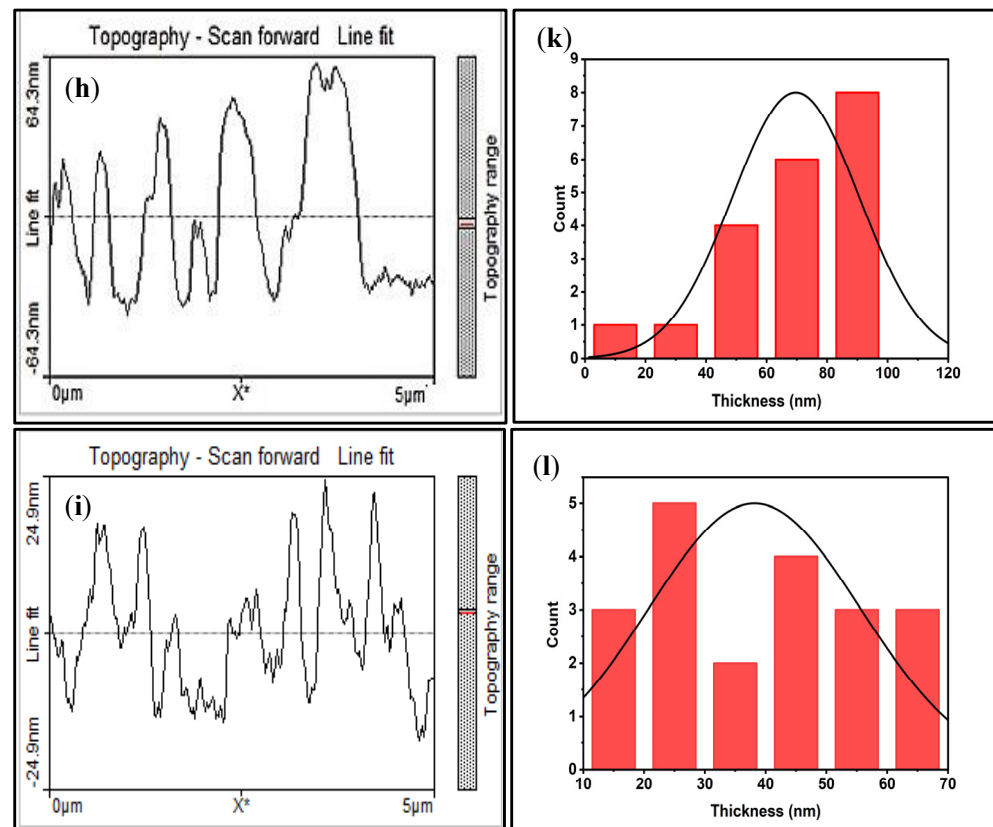


Figure 6. AFM images of (a,b) pristine MoS₂ NSs, (c,d) pristine BC, and (e,f) MoS₂-BC-3 NC; (g–i) height profiles and (j–l) thickness histograms at 5 μm scale of pristine MoS₂ NSs, pristine BC, and MoS₂-BC-3 NC. [X indicates the distance measured from 0 μm to 5 μm].

3.6. FESEM and EDX Analysis

The FESEM images reveal the morphological features and the EDX spectra provide the composition of the materials (Figure 7). FESEM images recorded at various magnifications showcase the micro- and nano-scale surface morphology of the MoS₂/BC3 NC, pristine MoS₂ NSs, and pristine BC. FESEM images of the pristine MoS₂ NSs show bundles of layered structures (Figure 7a–c) and the images of the pristine BC (Figure 7d–f) revealed thick sheet-like morphology with porosity. The FESEM images of the as-prepared MoS₂/BC3 NC with different magnifications (Figure 7g–i) show a scattered sheet-like morphology with MoS₂ (bright tiny spots) on the surface of the BC (dark regions).

The EDX spectra of pristine MoS₂ NSs show the presence of molybdenum and sulfur, whereas the pristine BC shows carbon, oxygen, calcium, and potassium. The as-prepared MoS₂/BC3 NC shows the presence of molybdenum, sulfur, carbon, oxygen, and aluminum (due to aluminum foil coating). The results provided proof of the incorporation of BC into the as-prepared MoS₂/BC3 NC (Figure 8a–c).

Thus, the spectroscopic, structural, and morphological studies confirm the synergistic interaction between MoS₂ and BC, which is well reflected in the facile exfoliation process, and the formation of few-layered MoS₂ NSs on the surface of the BC without any agglomeration.

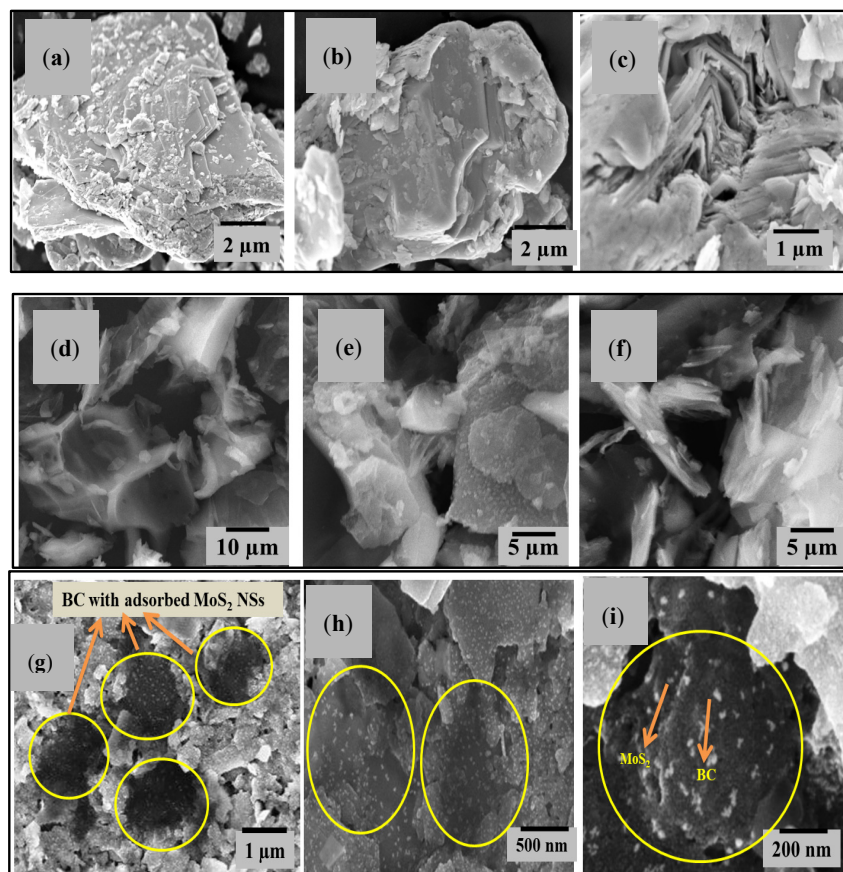


Figure 7. FESEM images of (a–c) pristine MoS₂ NSs, (d–f) pristine BC, and (g–i) MoS₂-BC₃ NC.

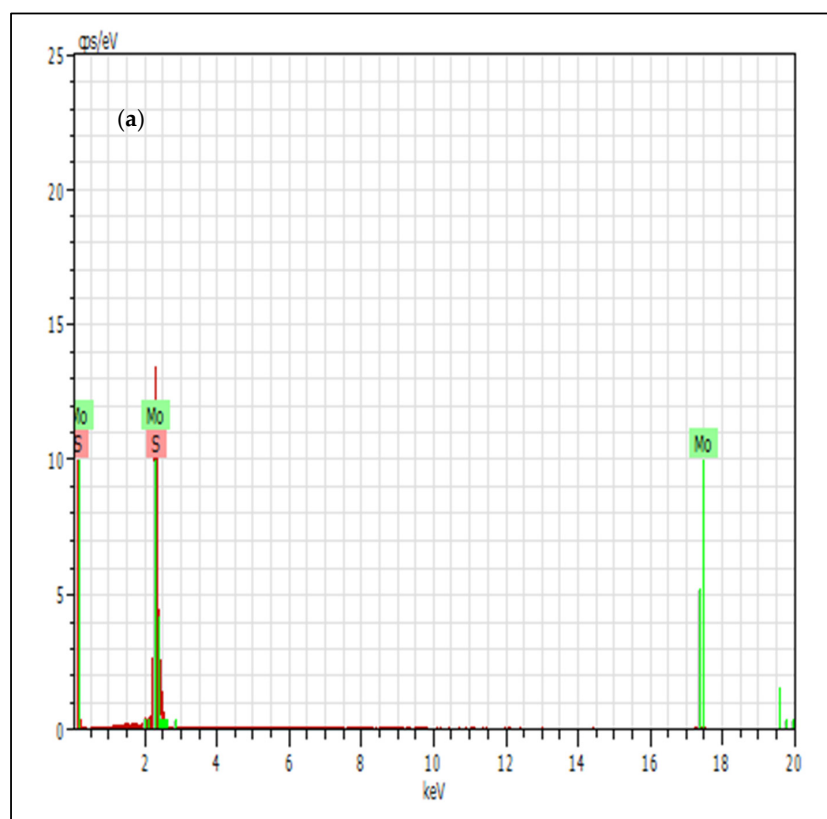


Figure 8. Cont.

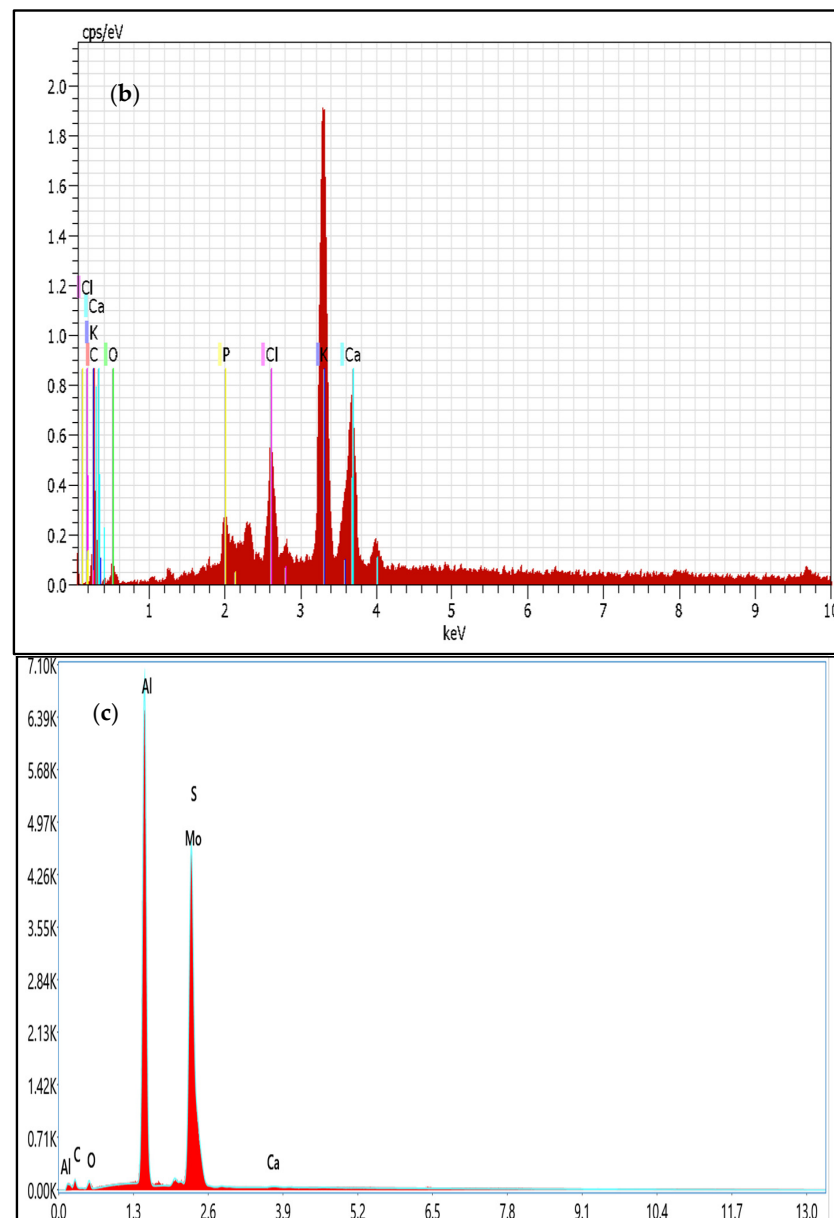


Figure 8. EDX spectra of (a) pristine MoS₂ NSs, (b) pristine BC, and (c) MoS₂-BC3 NC.

3.7. Electrochemical Analysis

3.7.1. EIS Analysis

The EIS technique was used to analyze the interfacial properties of the electrode material while it was in contact with the electrolyte solution. The EIS data are represented by Nyquist plots with real and imaginary parts of impedance at low- and high-frequency regions of the electrochemical system. At a higher frequency, the appearance of the semicircle region in the plots represents a high charge transfer resistance, which leads to poor electrical conductivity, and at a lower frequency, a diagonal line represents Warburg impedance due to the diffusion of ions. The electrical conductivity of MoS₂/BC1, MoS₂/BC2, MoS₂/BC3 NCs, pristine BC, pristine MoS₂ NSs, bulk BC, and bulk MoS₂ was examined using the charge transfer resistance (R_{ct}) and solution resistance (R_s) at an amplitude of 50 mV in the frequency range of 100 kHz to 0.1 Hz in 1 M H₂SO₄ (Figure 9). The R_s value was determined by the intercept of the real axis at a higher frequency and the R_{ct} value was obtained by measuring the distance from the high frequency intercept (R_s) to the low frequency intercept of the semicircle in the real axis of the Nyquist plots. The lower R_{ct} and R_s value

represents higher electrical conductivity, which facilitates the rapid movement of electrons for quick charge transfer reactions at the electrode and the electrolyte interface. The R_{ct} and R_s values of the prepared samples are represented in Table 2. The bulk MoS_2 and BC had higher charge transfer and solution resistance, which leads to poor electrical conductivity. However, upon exfoliating the bulk MoS_2 and BC, the formed pristine MoS_2 NSs and pristine BC exhibited comparatively low R_{ct} and R_s values. The prepared $\text{MoS}_2/\text{BC1}$, $\text{MoS}_2/\text{BC2}$, and $\text{MoS}_2/\text{BC3}$ NCs still exhibited lower R_{ct} and R_s values than the pristine counterparts. Among the three NCs, $\text{MoS}_2/\text{BC3}$ had a low charge transfer and solution resistance of 0.85 and 8.06 Ω , respectively; hence, it had higher electrical conductivity. Thus, the limitation of pristine MoS_2 in electrical conductivity due to its high charge transfer resistance is overcome by the gradual addition of BC into the NCs, which increases the number of active sites and the carbon network, thereby improving the charge transfer kinetics at the MoS_2 –BC interface, leading to the low impedance value of the NC compared to pristine materials.

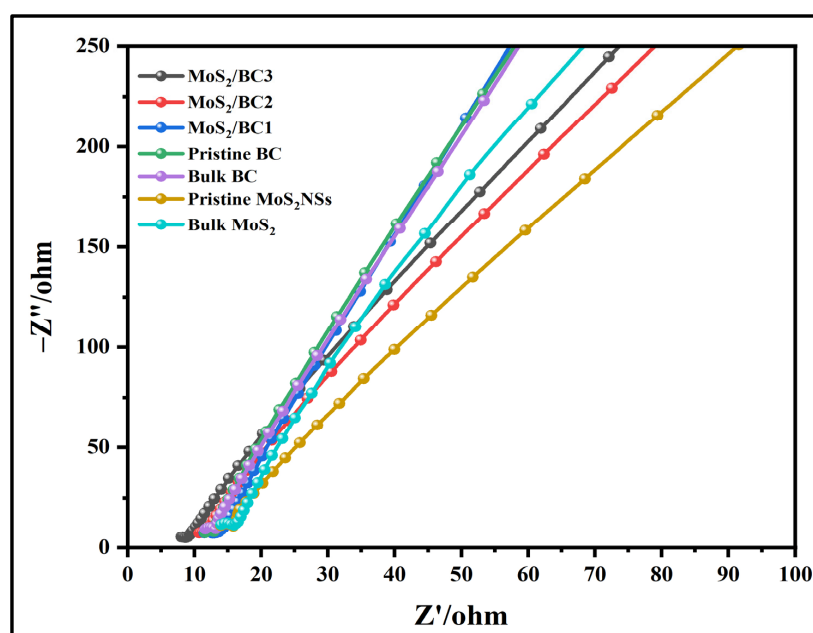


Figure 9. Nyquist plots of EIS for bulk MoS_2 , pristine MoS_2 NSs, bulk BC, pristine BC, $\text{MoS}_2/\text{BC1}$, $\text{MoS}_2/\text{BC2}$, and $\text{MoS}_2/\text{BC3}$ NCs.

Table 2. R_{ct} and R_s value of the prepared samples from the Nyquist plot.

Samples	R_{ct} (Ω)	R_s (Ω)
Bulk MoS_2	2.05	14.03
Pristine MoS_2 NSs	1.80	13.95
Bulk BC	1.54	11.65
Pristine BC	1.30	11.59
$\text{MoS}_2/\text{BC1}$	1.19	11.48
$\text{MoS}_2/\text{BC2}$	1.01	10.71
$\text{MoS}_2/\text{BC3}$	0.7	8.06

3.7.2. CV Analysis

The CV technique was used to study the electrochemical properties and redox behavior of the modified electrode surfaces. Since $\text{MoS}_2/\text{BC3}$ NC shows low charge transfer resistance and solution resistance, the CV profile of the GCE-modified electrode with $\text{MoS}_2/\text{BC3}$ was recorded and compared with the pristine BC and pristine MoS_2 NSs in 0.1 M KCl containing 5 mM of $\text{Fe}(\text{CN})_6^{3-/4-}$ at different scan rates (20, 40, 60, 80, and 100 mVs^{-1}) (Figure 10a–c). The current response of CV enhances when increasing the scan

rate due to rapid diffusion of the analytes at a faster scan rate. A linear relationship between the anodic and cathodic peak currents at different scan rates indicates a diffusion-controlled reaction of the prepared electrode material. The surface area of the modified electrodes was calculated using the peak current from the redox reactions of $\text{Fe}(\text{CN})_6^{3-/4-}$ at a scan rate of 50 mV/s using the diffusion coefficient values in the Randles–Ševčík equation. The calculated electrochemical surface areas for the $\text{MoS}_2/\text{BC3 NC}$, pristine BC, and pristine MoS_2 NSs are 0.074, 0.07, and 0.069 cm^2 , respectively. The result shows that the incorporation of highly porous and amorphous BC prevents restacking of the layered MoS_2 NSs, thereby increasing the surface area which in turn increases the peak current of the $\text{MoS}_2/\text{BC3 NC}$ s by providing more active sites for electrochemical reactions.

The capacitive behavior of the prepared materials was analyzed by recording the CV profiles of the modified electrodes with $\text{MoS}_2/\text{BC3 NC}$, pristine BC, and pristine MoS_2 NSs in the potential window of 0–0.5 V at different scan rates (20, 40, 60, 80, and 100 mVs^{-1}) in 1 M H_2SO_4 . The $\text{MoS}_2/\text{BC3}$ and pristine BC-modified electrodes display quasi rectangular CV curves due to the presence of both the electric double layer and the pseudo capacitive behavior of the modified electrodes. The CV curve of pristine MoS_2 NSs shows a pair of faradaic redox peaks due to the electron transfer across the electrode–electrolyte interface, representing the pseudocapacitive nature of pristine MoS_2 NSs (Figure 11a–c). The dual structural property of highly porous pristine BC and the layered structure of MoS_2 NSs in the $\text{MoS}_2/\text{BC3 NC}$ increased the overall area of the curve, which in turn increased the specific capacitance. The specific capacitance values calculated from the CV curve for the modified electrodes at different scan rates are listed in Table 3. The $\text{MoS}_2/\text{BC3 NC}$ had a higher specific capacitance value of 34 F/g than pristine MoS_2 NSs and pristine BC at a scan rate of 20 mVs^{-1} . At lower scan rates, the specific capacitance increased due to the diffusion of a large number of electrolytic ions into the pores of the electrode material over an extended period. The electrochemical studies reiterate the synergy between MoS_2 and BC in terms of the improved overall surface areas, electrical conductivity, capacitive behavior, and specific capacitance values. While BC offers electric double-layer capacitance, MoS_2 NSs exhibit faradaic pseudocapacitance and when present together, the NC is more suitable for the development of an electrode material for hybrid capacitors.

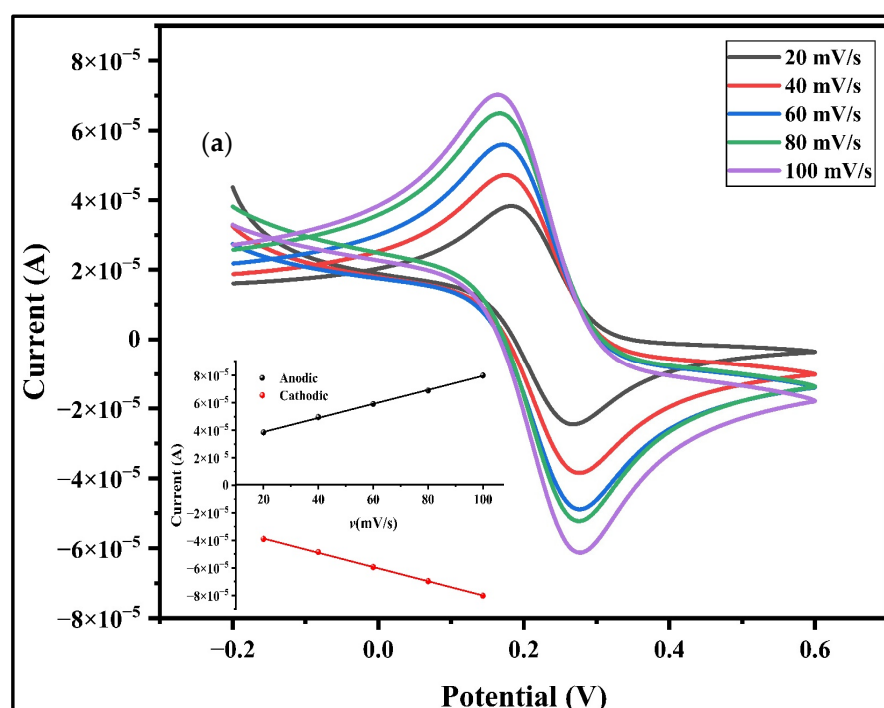


Figure 10. Cont.

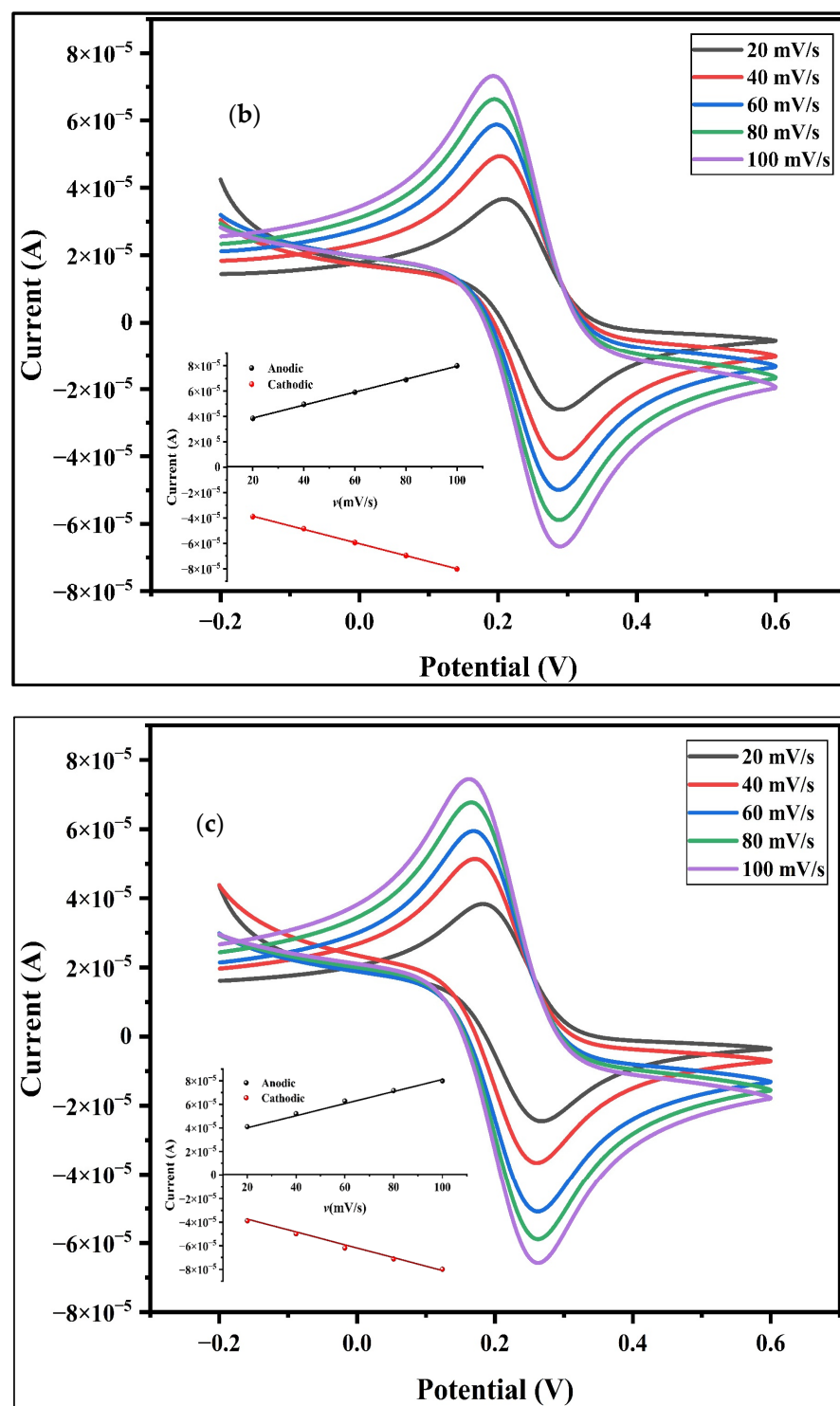


Figure 10. CV profiles for (a) pristine MoS_2 NSs, (b) pristine BC, and (c) MoS_2 -BC3 NC in 0.1 M KCl containing 5 mM of $\text{Fe}(\text{CN})_6^{3-/4-}$. Inset shows the linear plot of scan rate (v) vs. anodic (I_{pa}) and cathodic (I_{pc}) peak currents.

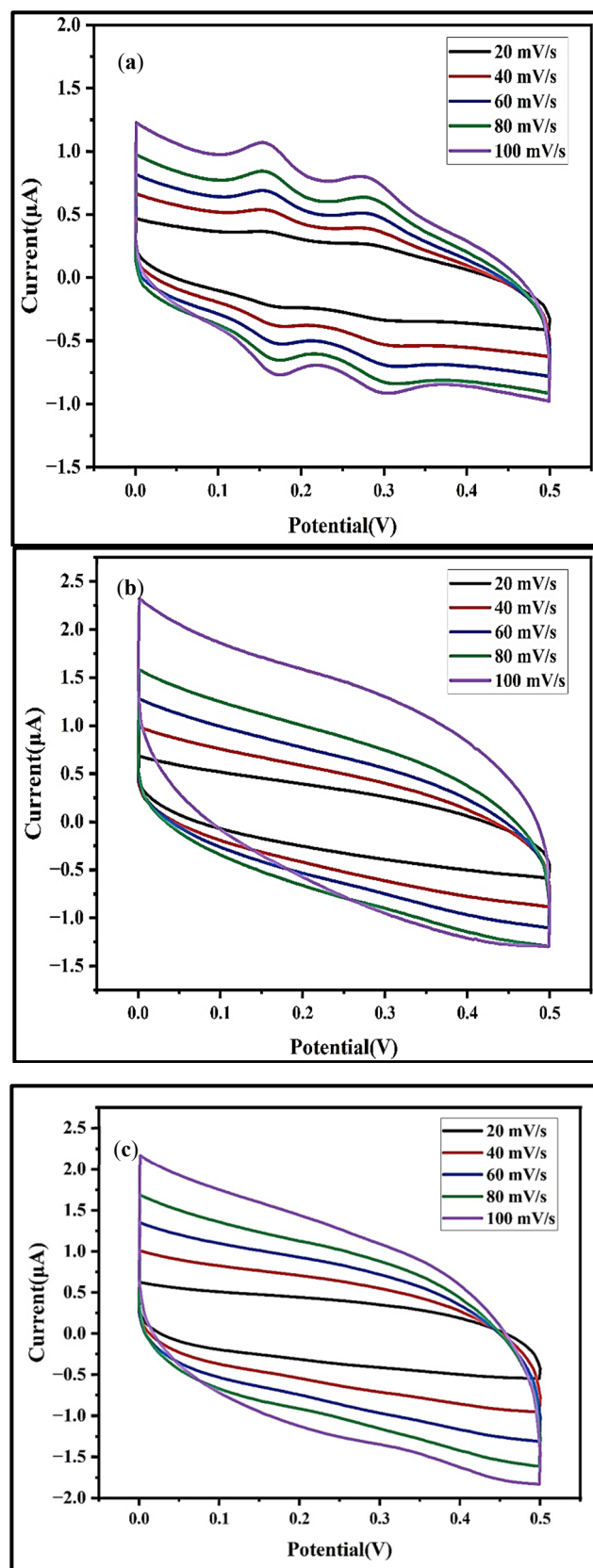


Figure 11. CV profiles of (a) pristine MoS_2 NSs, (b) pristine BC, and (c) MoS_2 -BC3 NC in 1 M H_2SO_4 .

Table 3. Specific capacitance of the pristine MoS₂ NSs, pristine BC, and MoS₂/BC3 NC from the CV curve at different scan rates.

Scan Rate (mVs ^{−1})	Specific Capacitance (F/g)		
	Pristine MoS ₂ NSs	Pristine BC	MoS ₂ /BC3 NC
100	14.89	21.56	22.8
80	15.83	20.83	23.5
60	17.03	21.85	25.5
40	19.44	25.0	28.5
20	25.56	31.11	34

4. Conclusions

In conclusion, we have successfully investigated and revealed the synergistic effect of an MoS₂ NSs/BC nanocomposite through spectroscopic, structural, and electrochemical studies, and have proven the ability of the NC to be used for energy storage applications. The presence of BC prevents the agglomeration of MoS₂ NSs, resulting in the formation of few-layered NSs through adsorption of the formed NSs onto the surface of the BC. Also, the amorphous and porous nature of BC helps to improve the surface area of the NC, which in turn enhances electrochemical properties like the electrical conductivity and specific capacitance of the NC-modified electrode on the GC surface. Interestingly, PL studies reveal a substantial increase in the luminescence characteristics of NC compared to the less luminescent bulk BC and non-luminescent bulk MoS₂. Thus, the prepared MoS₂/BC NCs offer ample scope for further improvement and development for energy storage and photoluminescence applications.

Author Contributions: Data curation, conceptualization and design, analysis and interpretation of data, reviewing and editing draft, V.S. Acquisition of data, analysis and interpretation of data, data curation, writing and revising the draft, T.P. Acquisition of data, analysis and interpretation of data, data curation, writing and revising the draft, C.P. Editing and revising the draft, B.A.V.M. and M.K. All authors have read and agreed to the published version of the manuscript.

Funding: This research received no external funding.

Data Availability Statement: Requested data can be provided.

Acknowledgments: The authors T.P., C.P., and V.S. acknowledge the facilities provided by the Science Instrumentation Centre, Lady Doak College, Madurai, which was established and funded by University Grants Commission and the Department of Science and Technology, India, for facilitating the present work.

Conflicts of Interest: The authors declare no conflicts of interest.

References

- Öztürk, O.; Gür, E. Layered transition metal sulfides for supercapacitor applications. *ChemElectroChem* **2024**, *11*, e202300575. [\[CrossRef\]](#)
- Cook, J.B.; Kim, H.S.; Lin, T.C.; Lai, C.H.; Dunn, B.; Tolbert, S.H. Pseudocapacitive charge storage in thick composite MoS₂ nanocrystal-based electrodes. *Adv. Energy Mater.* **2017**, *7*, 1601283. [\[CrossRef\]](#)
- Li, X.; Wang, J.; Xie, D.; Xu, J.; Xia, Y.; Xiang, L.; Komarneni, S. Reduced graphene oxide/MoS₂ hybrid films for room-temperature formaldehyde detection. *Mater. Lett.* **2017**, *189*, 42–45. [\[CrossRef\]](#)
- Abdel Maksoud, M.I.A.; Bedir, A.G.; Bekhit, M.; Abouelela, M.M.; Fahim, R.A.; Awed, A.S.; Rooney, D.W. MoS₂-based nanocomposites: Synthesis, structure, and applications in water remediation and energy storage: A review. *Environ. Chem. Lett.* **2021**, *19*, 3645–3681. [\[CrossRef\]](#)
- Bello, I.T.; Oladipo, A.O.; Adedokun, O.; Dhlamini, S.M. Recent advances on the preparation and electrochemical analysis of MoS₂-based materials for supercapacitor applications: A mini-review. *Mater. Today Commun.* **2020**, *25*, 101664. [\[CrossRef\]](#)

6. Ismail, K.B.M.; Arun Kumar, M.; Mahalingam, S.; Kim, J.; Atchudan, R. Recent advances in molybdenum disulfide and its nanocomposites for energy applications: Challenges and development. *Materials* **2023**, *16*, 4471. [\[CrossRef\]](#)
7. Zheng, L.; Xing, T.; Ouyang, Y.; Wang, Y.; Wang, X. Core-shell structured MoS₂@Mesoporous hollow carbon spheres nanocomposite for supercapacitors applications with enhanced capacitance and energy density. *Electrochim. Acta* **2019**, *298*, 630–639. [\[CrossRef\]](#)
8. Wang, L.; Liu, F.; Zhao, B.; Ning, Y.; Zhang, L.; Bradley, R.; Wu, W. Carbon nanobowls filled with MoS₂ nanosheets as electrode materials for supercapacitors. *ACS Appl. Nano Mater.* **2020**, *3*, 6448–6459. [\[CrossRef\]](#)
9. da Silveira Firmiano, E.G.; Rabelo, A.C.; Dalmaschio, C.J.; Pinheiro, A.N.; Pereira, E.C.; Schreiner, W.H.; Leite, E.R. Supercapacitor electrodes obtained by directly bonding 2D MoS₂ on reduced graphene oxide. *Adv. Energy Mater.* **2014**, *4*, 1301380. [\[CrossRef\]](#)
10. Chen, P.S.; Hu, Y.; Li, S.Y.; Mazurkiewicz-Pawlicka, M.; Małolepszy, A. Preparation of a MoS₂/carbon nanotube nanocomposite by hydrothermal method for supercapacitor. *Int. J. Electrochem. Sci.* **2024**, *19*, 100523. [\[CrossRef\]](#)
11. Das, R.; Panda, S.N. Preparation and applications of biocharbased nanocomposite: A review. *J. Anal. Appl. Pyrolysis* **2022**, *167*, 105691. [\[CrossRef\]](#)
12. Zhao, G.; Cheng, Y.; Sun, P.; Ma, W.; Hao, S.; Wang, X.; Liu, M. Biocarbon based template synthesis of uniform lamellar MoS₂ nanoflowers with excellent energy storage performance in lithium-ion battery and supercapacitors. *Electrochim. Acta* **2020**, *331*, 135262. [\[CrossRef\]](#)
13. Sangeetha, D.N.; Selvakumar, M. Active-defective activated carbon/MoS₂ composites for supercapacitor and hydrogen evolution reactions. *Appl. Surf. Sci.* **2018**, *453*, 132–140. [\[CrossRef\]](#)
14. Khandare, L.N.; Late, D.J.; Chaure, N.B. MoS₂ nanobelts-carbon hybrid material for supercapacitor applications. *Front. Chem.* **2023**, *11*, 1166544. [\[CrossRef\]](#) [\[PubMed\]](#)
15. Mahajan, H.; Mohanan, K.U.; Cho, S. Facile synthesis of biocarbon-based MoS₂ composite for high-performance supercapacitor application. *Nano Lett.* **2022**, *22*, 8161–8167. [\[CrossRef\]](#)
16. Wang, F.; Ma, J.; Zhou, K.; Li, X. MoS₂/corncob-derived activated carbon for supercapacitor application. *Mater. Chem. Phys.* **2020**, *244*, 122215. [\[CrossRef\]](#)
17. Yang, Z.; Xing, R.; Zhou, W.; Zhu, L. Adsorption characteristics of ciprofloxacin onto g-MoS₂ coated biochar nanocomposites. *Front. Environ. Sci. Eng.* **2020**, *14*, 1–10. [\[CrossRef\]](#)
18. Zhu, J.; Yan, L.; Li, X.; Song, W.; Yan, T.; Li, Y. Ball-milled MoS₂/biochar as peroxymonosulfate activator efficiently removes tetracycline: Multiple active sites-triggered radical/non-radical pathways. *Ind. Crops Prod.* **2023**, *205*, 117450. [\[CrossRef\]](#)
19. Zhu, H.; Tan, X.; Tan, L.; Chen, C.; Alharbi, N.S.; Hayat, T.; Wang, X. Biochar derived from sawdust embedded with molybdenum disulfide for highly selective removal of Pb²⁺. *ACS Appl. Nano Mater.* **2018**, *1*, 2689–2698. [\[CrossRef\]](#)
20. Khan, Z.H.; Gao, M.; Qiu, W.; Song, Z. Mechanism of novel MoS₂-modified biochar composites for removal of cadmium (II) from aqueous solutions. *Environ. Sci. Pollut. Res.* **2021**, *28*, 34979–34989. [\[CrossRef\]](#)
21. Gusain, R.; Kumar, N.; Fosso-Kankeu, E.; Ray, S.S. Efficient removal of Pb (II) and Cd (II) from industrial mine water by a hierarchical MoS₂/SH-MWCNT nanocomposite. *ACS Omega* **2019**, *4*, 13922–13935. [\[CrossRef\]](#) [\[PubMed\]](#)
22. Tomy, M.; Anu, M.A.; Xavier, T.S. Effect of chemical exfoliation on the specific capacitance of MoS₂ decorated conducting polymer electrodes for supercapacitor applications. *Appl. Phys. A* **2023**, *129*, 818. [\[CrossRef\]](#)
23. Jawaid, A.; Nepal, D.; Park, K.; Jespersen, M.; Qualley, A.; Mirau, P.; Vaia, R.A. Mechanism for liquid phase exfoliation of MoS₂. *Chem. Mater.* **2016**, *28*, 337–348. [\[CrossRef\]](#)
24. Gan, X.; Zhao, H.; Wong, K.Y.; Lei, D.Y.; Zhang, Y.; Quan, X. Covalent functionalization of MoS₂ nanosheets synthesized by liquid phase exfoliation to construct electrochemical sensors for Cd (II) detection. *Talanta* **2018**, *182*, 38–48. [\[CrossRef\]](#)
25. Ma, H.; Ben, S.; Shen, Z.; Zhang, X.; Wu, C.; Liao, S.; An, F. Investigating the exfoliation behavior of MoS₂ and graphite in water: A comparative study. *Appl. Surf. Sci.* **2020**, *512*, 145588. [\[CrossRef\]](#)
26. Eltaweil, A.S.; Abdelfatah, A.M.; Hosny, M.; Fawzy, M. Novel biogenic synthesis of a Ag@ Biochar Nanocomposite as an antimicrobial agent and photocatalyst for methylene blue degradation. *ACS Omega* **2022**, *7*, 8046–8059. [\[CrossRef\]](#)
27. Li, M.; Zhang, A.; Wu, H.; Liu, H.; Lv, J. Predicting potential release of dissolved organic matter from biochars derived from agricultural residues using fluorescence and ultraviolet absorbance. *J. Hazard. Mater.* **2017**, *334*, 86–92. [\[CrossRef\]](#)
28. Al-Mashat, L.; Shin, K.; Kalantar-Zadeh, K.; Plessis, J.D.; Han, S.H.; Kojima, R.W.; Wlodarski, W. Graphene/polyaniline nanocomposite for hydrogen sensing. *J. Phys. Chem. C* **2010**, *114*, 16168–16173. [\[CrossRef\]](#)
29. Lee, C.; Yan, H.; Brus, L.E.; Heinz, T.F.; Hone, J.; Ryu, S. Anomalous lattice vibrations of single-and few-layer MoS₂. *ACS Nano* **2010**, *4*, 2695–2700. [\[CrossRef\]](#)
30. Mahdavi, M.; Kimiagar, S.; Abrinaei, F. Preparation of few-layered wide bandgap MoS₂ with nanometer lateral dimensions by applying laser irradiation. *Crystals* **2020**, *10*, 164. [\[CrossRef\]](#)
31. Kandhasamy, D.M.; Muthu Mareeswaran, P.; Chellappan, S.; Namasivayam, D.; Aldahish, A.; Chidambaram, K. Synthesis and photoluminescence properties of MoS₂/graphene heterostructure by liquid-phase exfoliation. *ACS Omega* **2021**, *7*, 629–637. [\[CrossRef\]](#) [\[PubMed\]](#)

32. Castellanos-Gomez, A.; van der Zant, H.S.; Steele, G.A. Folded MoS₂ layers with reduced interlayer coupling. *Nano Res.* **2014**, *7*, 572–578. [[CrossRef](#)]
33. Shapira, K.; Zucker, I. Emerging investigator series: Molybdenum disulfide-enabled activated carbon-a multifunctional adsorbent for practical water treatment applications. *Environ. Sci. Nano* **2022**, *9*, 477–488. [[CrossRef](#)]

Disclaimer/Publisher’s Note: The statements, opinions and data contained in all publications are solely those of the individual author(s) and contributor(s) and not of MDPI and/or the editor(s). MDPI and/or the editor(s) disclaim responsibility for any injury to people or property resulting from any ideas, methods, instructions or products referred to in the content.